Prompt Fission Neutrons and Gamma Rays (Experiments)

F.-J. Hambsch
EC-JRC-Directorate G, Unit G.2
B-2440 Geel
Belgium

Introduction

The complex nuclear fission process is even after almost 80 years since its discovery still not understood in all details. Fission is a very fast process and fission fragment de-excitation takes place at a very early stage after scission through the successive emission of neutrons and γ-rays (see the schematic in Fig. 1). It involves a number of mechanisms which are reflected in the properties of fission observables. These observables and in particular those associated with prompt fission neutron and γ-ray emission govern the performances of applied nuclear systems.
In nuclear applications the multiplicity of prompt neutrons and γ-rays as well as their energy release are crucial numbers which need to be known with high precision. In this manuscript the focus is on prompt emission and delayed decays are neglected.
Properties of the emitted particles are important for the better understanding of the mechanism of fission fragment de-excitation. Precise experimental data on prompt fission neutron and γ-ray emission, e.g. multiplicity, average energy per particle and total dissipated energy per fission, preferably as a function of fission-fragment mass and total kinetic energy, are key input to benchmark nuclear fission models attempting to describe the competition between prompt neutron and γ-ray emission.

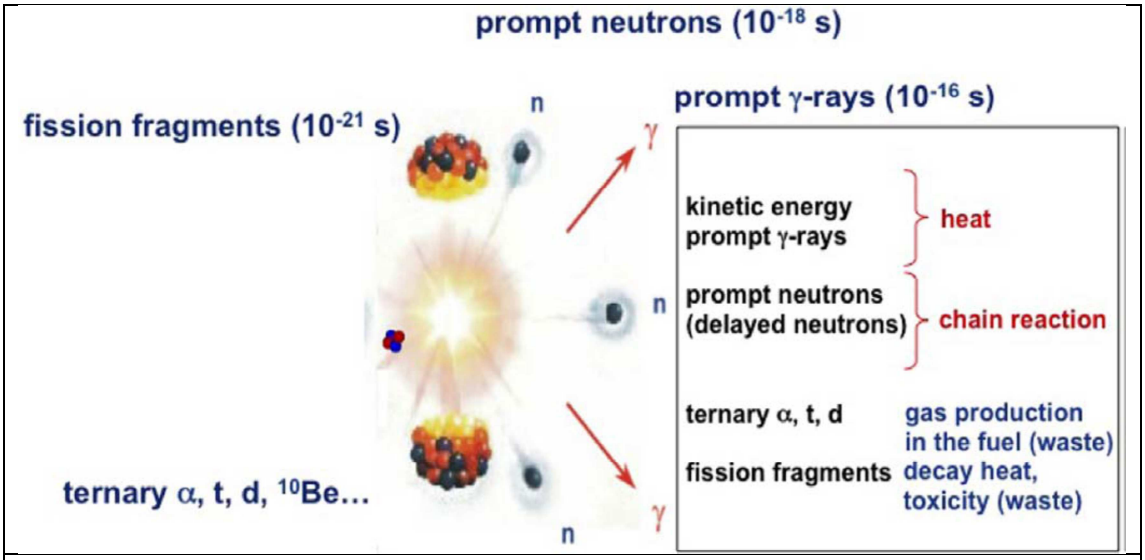

Fig. 1. The fission process including timings (from Ref. [1]).

Prompt neutron and γ-emission in fission is governed by the excitation energy of the fission fragments. Since we consider here only neutron and γ-ray emission after scission, the neutron and γ-ray multiplicity is a direct consequence of the energy stored in the nascent fragments at scission. This could be in form of collective excitation energy or deformation energy. Hence the variation of the neutron yield with fission fragment properties like mass distribution, compound nuclear excitation energy or kinetic energy release is an important quantity to understand e.g. the energy partition at scission.

On average 2-4 neutrons are released and about 6-10 γ-rays. The exact values of those released particles are of course dependent on the isotope under investigation and on the excitation energy of the compound nucleus. The average energy of the emitted neutrons in the laboratory system is about 2 MeV and those of the γ-rays about 7-9 MeV.
For applications in nuclear energy average quantities like average neutron multiplicity as a function of incident neutron energy are of importance and need to be known to a very high precision.
In the following two chapters we will concentrate on the experimental part of prompt neutron and γ-ray measurements and highlight some results.

Prompt fission neutron emission

In general neutrons are more difficult to detect than γ-rays because of their weak interaction with matter and their large dynamic range in energy. The material with which neutrons are being detected needs to have a high cross section for neutron interaction. In Fig. 2 the most important isotopes with high neutron capture cross sections are given. Amongst them is hydrogen.

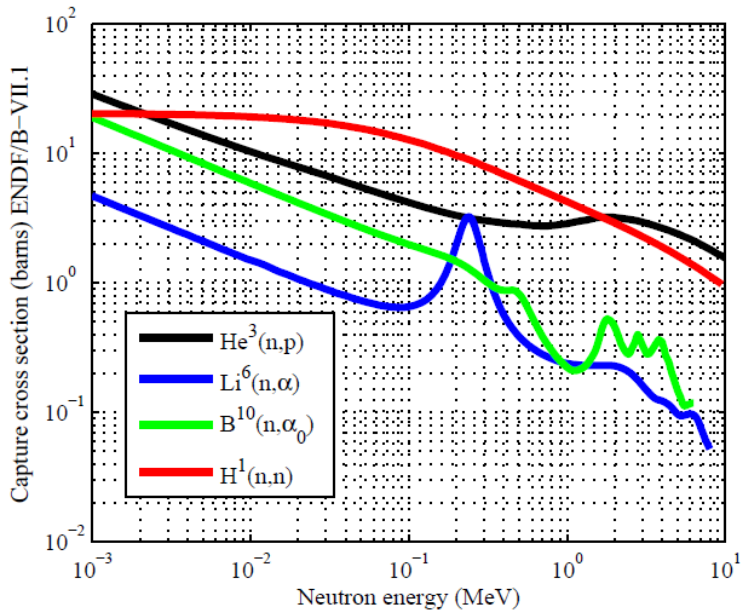

Fig. 2. Capture cross sections for typical neutron absorbers (image from Ref. [2]).

Fast neutrons can interact with materials that contain a large concentration of hydrogen atoms (protons), in e.g. organic material, due to elastic scattering in which case the energy of the neutron is (partially) transferred to the protons which in turn can produce scintillation light. Using the above principle, fast neutrons can be detected in any organic (plastic or liquid) scintillator.
The efficiency of neutron absorption in a liquid scintillator can be increased by adding 0.5% by weight of Gadolinium to the liquid. Gd has also a very high neutron capture cross section.
For the measurement of neutron probability or neutron multiplicity distributions a large neutron detection apparatus with very high fission neutron detection efficiency is required. In Fig. 3 a typical tank based neutron multiplicity detector is shown [3].

Spontaneous fission and thermal neutron induced fission neutron multiplicity distributions have been measured for a large number of heavy nuclei [4-7]. The high neutron detector efficiency needed to make neutron multiplicity distribution measurements, causes significant background problems in the case of non-thermal neutron induced reactions. This is because the incident neutrons can scatter from fission chambers and shielding materials into the neutron detector. The measurement of neutron multiplicity distributions in non-thermal neutron induced fission reactions is thus very difficult. To my knowledge there is only a single set of such measurements on ^{235}U, ^{238}U, and ^{239}Pu in the incident neutron energy range from 1 to 15 MeV [8].
Multiplicity counters can also be based on ^{3}He tubes embedded in a polyethylene enclosure (see Fig. 4) [9].

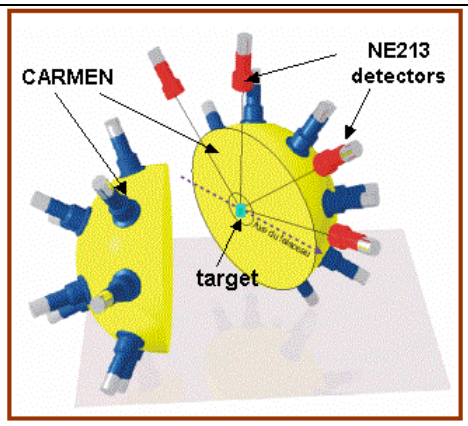

Fig. 3. The CARMEN liquid scintillation detector. Details are given in Ref. [3].

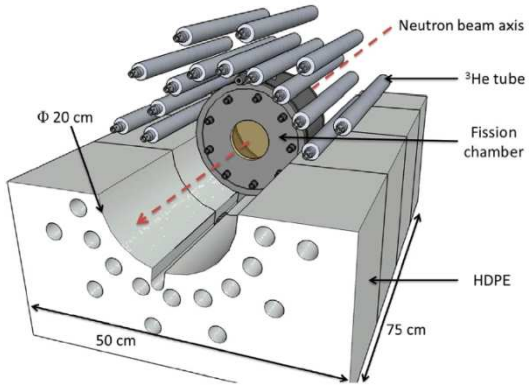

Fig. 4. A ^{3}He tube based detector system. Details are given in Ref. [9].

Neutron detectors based on organic (plastic or liquid) scintillation material are widely used in fission research. Their range of application covers nearly all the topics in basic and applied nuclear research. They are very well suited to study correlation of prompt neutron emission with fission fragments properties.
In contrast to the just mentioned Gd-loaded scintillator tanks or ^{3}He tube arrays, in some liquid scintillators fast neutrons produce scintillations with different decay times for neutrons and γ-rays.
The prompt decay time is typically a couple of nanoseconds, while the delayed decay time is normally on the order of hundreds of nanoseconds. The majority of the light is produced by the prompt decay; however, the amount of light in the delayed component often varies as a function of the type of particle causing the excitation [10]. The variation in the amount of light produced by delayed fluorescence can be used to distinguish different types of particles. Using this Pulse Shape Discrimination (PSD) technique, it is therefore possible to separate fast neutrons from γ-rays. Fig. 5 illustrates this effect.

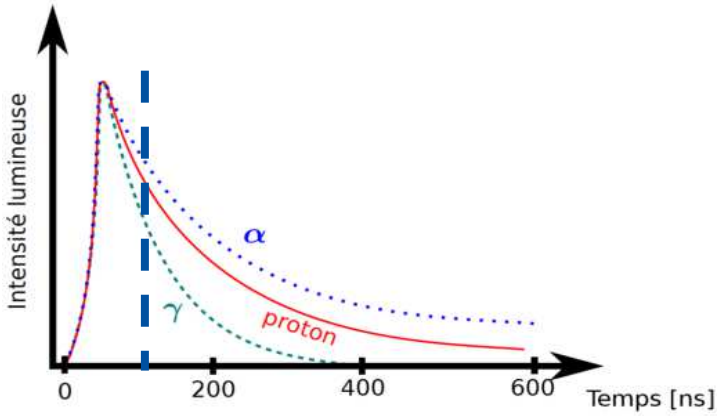

Fig. 5. Typical time distribution of a liquid scintillation detector which allows pulse shape discrimination. Image taken from Ref. [11].

A typical two-dimensional distribution of the pulse shape discrimination (PSD) signal versus the light output is shown in Fig. 6. It is clear from this figure that there will be a detection threshold below which it will be impossible to discriminate between neutrons and γ-rays. The threshold is typically between 300-500 keV neutron energy. To detect neutrons below this threshold ^{6}Li containing scintillation materials is used. In this reaction, a triton and an alpha particle are produced. One of the problems is the rather low detection efficiency and the fact that there is no threshold and hence the detector is very sensitive to background neutrons.

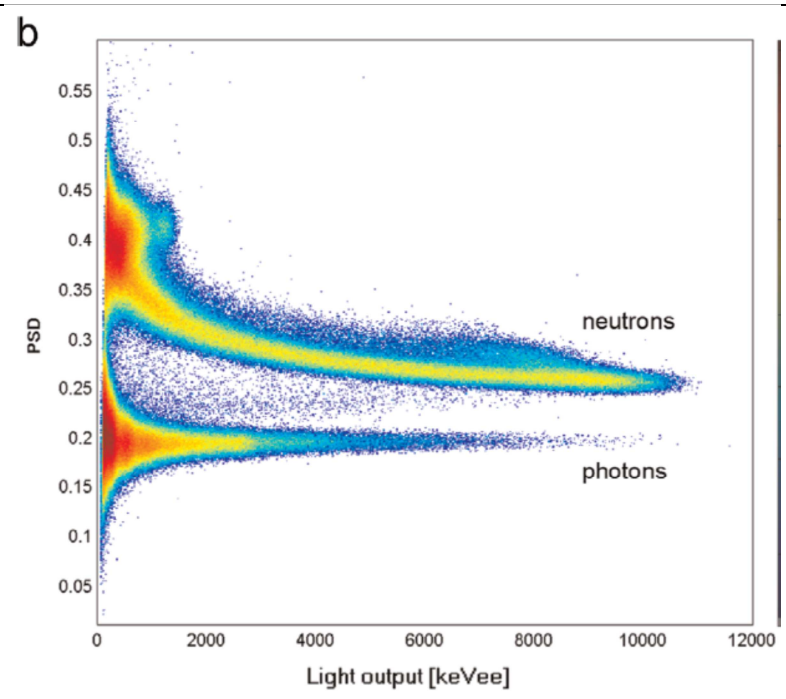

Fig.6 Two-parameter plot of PSD versus light output for the BC-501 [12].

However, before any useful information can be determined by using either ^{6}Li-glass or organic scintillation detectors the response to neutrons and γ-rays of those detectors needs to be determined. This is being done by measuring the response function using

mono-energetic neutron beams and γ-ray sources to cover an incident energy range of say up to 10 MeV and beyond. GEANT4 [13] is nowadays used as a toolkit to simulate the detector response and then be compared to the measured response. Also the Monte Carlo code GRESP [14] is used to calculate the theoretical Compton distributions for the γ-ray sources used in the calibration procedure. A typical result is shown in Fig. 7

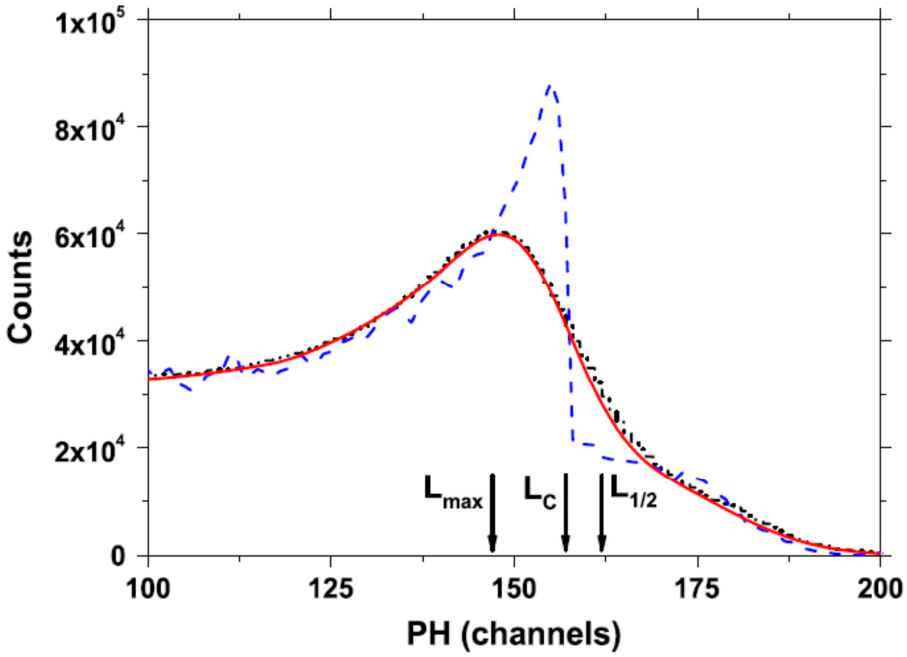

Fig. 7. The pulse height (PH) spectrum from a ^{137}Cs source (dotted line), the GRESP generated Compton spectrum (dashed line) and the folded spectrum (full line). L_C represents the position of the Compton edge; L_{max} and $L_{1/2}$ represent the channel position of the peak maximum and half maximum, respectively. Image taken from Ref. [15].

The energy calibration of organic scintillators is often difficult with γ-ray sources as photons up to 3 MeV interact by Compton scattering and the position of the Compton edge is strongly influenced by the photon energy and detector resolution.
An empirical formula to determine the detector resolution was presented by Dietze and Klein [14].

$$\frac{\Delta E}{E} = 1.5\,\frac{L_{1/2}-L_{max}}{L_{1/2}} \qquad (1)$$

The resolution is directly proportional to the relative difference between the channel position of the maximum and half maximum height. A very good estimate of the detector resolution which is independent of the photon energy and the detector size could be calculated as given in eq. (1).
The response function of a neutron detector is determined by sorting the data into a calibrated PH vs. time-of-flight (TOF) matrix and selecting the desired neutron energies. The light output function for protons is constructed by determining the position of the most energetic protons for a given neutron energy [15]. This position, which in an ideal detector is a hard edge, is smeared by the resolution of the detector (see Figs. 7, 8). The high-energy minimum of the first derivative of the response function is the energy position of the most energetic protons. Typical response functions are given in Fig. 8. More details can be found in refs. [15, 16].

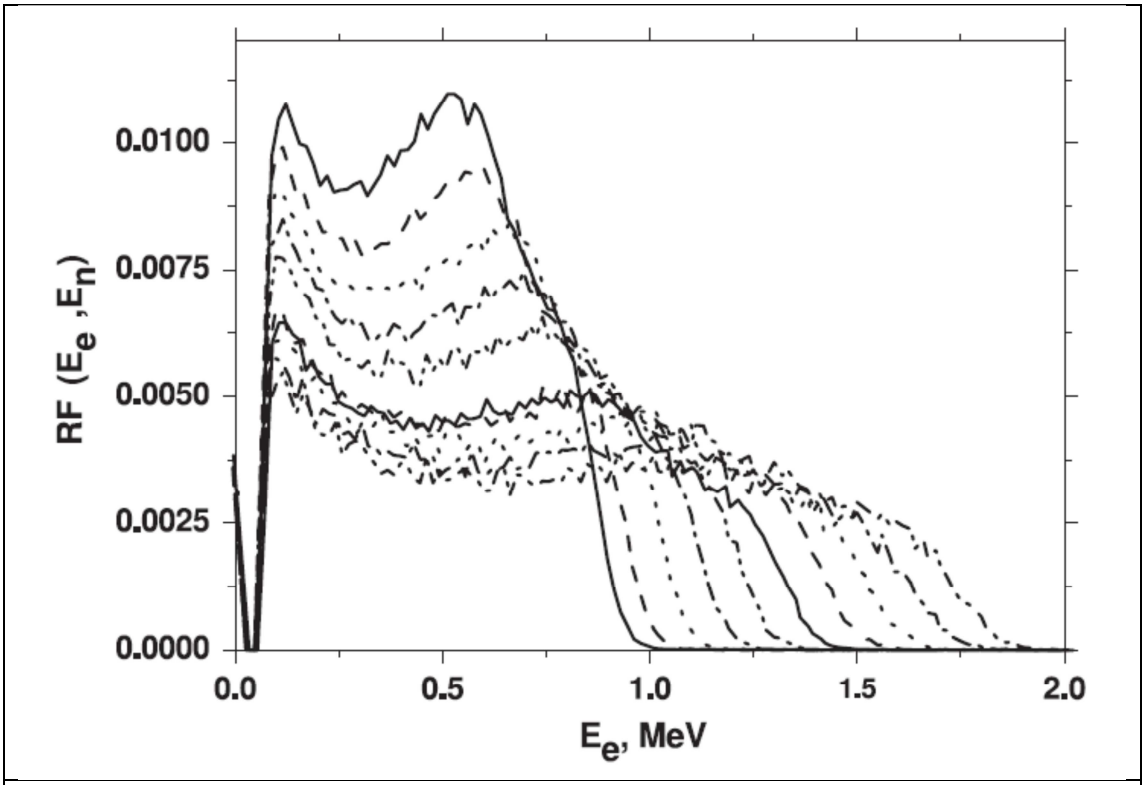

Fig. 8. Experimental response functions for neutron energies from 1.2 to 7 MeV, taken from Ref. [16].

Another technique to measure the energy of prompt neutron emission from fission is to use time-of-flight which consists of an accurate determination of the moment of emission of the neutron and detection in a fast plastic or liquid scintillator.

The moment of emission of the neutron is often determined with an (or many) active sample(s) inside an ionisation chamber. Since only thin targets can be used normally a multi-layer ionisation camber is used to improve the sample mass. Also many neutron detectors are used in form of an array to boost efficiency. A typical setup of such kind is the Chi-nu array at Los Alamos National Laboratory (LANL) [17]. This setup is designed to improve on the prompt fission neutron spectrum as a function of incident neutron energy for major actinides.

A similar approach however using a single target inside a modified and position sensitive ionisation chamber is followed at JRC-Geel [18]. Fig. 9 shows a sketch of the neutron detection and the ionisation chamber inside the SCINTIA array.

The setup is being used to investigate correlations between fission fragments and prompt neutron emission for major actinides as a function of incident neutron energy in the resonance region. A presentation of those results is outside of the scope of this paper but the acquired data have also been summed up in the incident neutron energy range of 0.3 eV to 60 keV which corresponds to an average incident neutron energy of a few keV and then compared to literature data of neutron induced fission of ^{235}U at thermal incident energy.

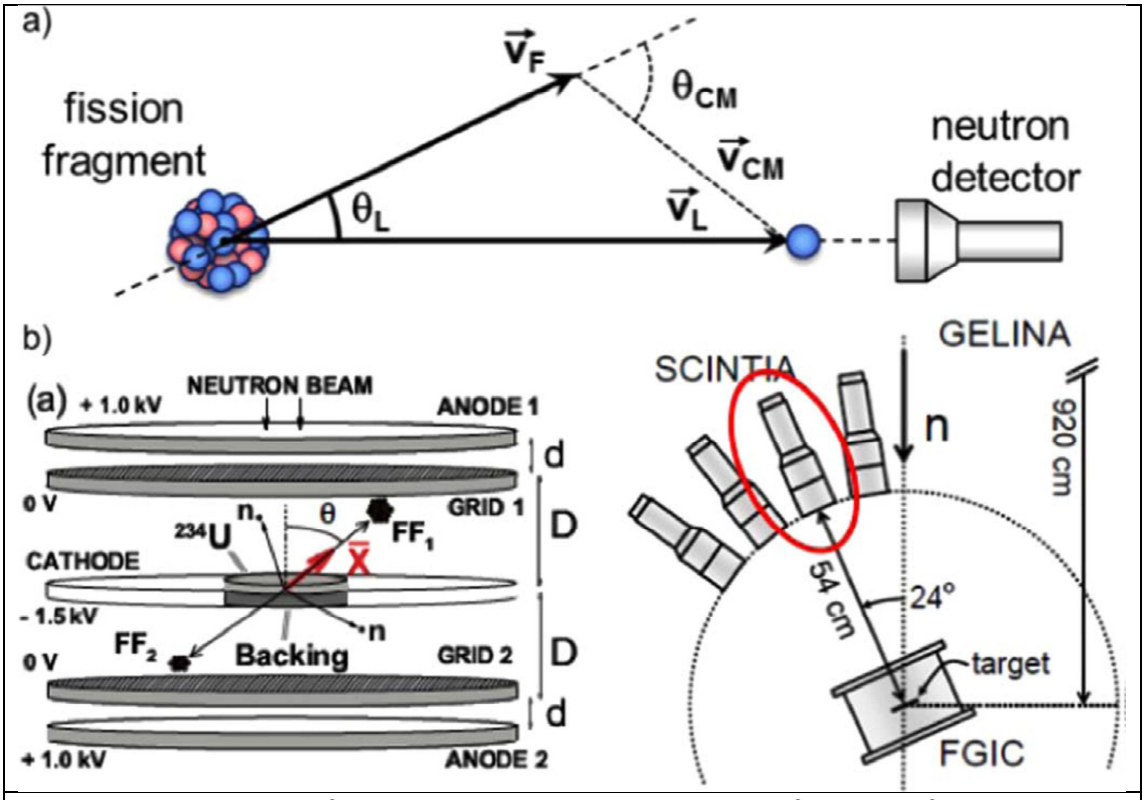

Fig. 9. (a) Kinematics of prompt neutron emission and transformation from laboratory system into centre-of-mass frame; (b) Sketch of a double Frisch-grid ionization chamber (FGIC) for fission-fragment measurements (left) and the arrangement of various neutron detectors relative to the FGIC and the incoming neutron beam (right); the detector indicated by the red circle is placed along the chamber symmetry axis and represents the traditional arrangement to obtain emission data in the centre-of-mass frame. Image taken from Ref. [1].

A closer look has shown some shortcomings in the present literature data. It has been a long lasting struggle for the theoretical understanding of the fission process to cope with the literature data on the neutron multiplicity as a function of the total kinetic energy (TKE) of the fission fragments.

As seen in Fig. 10 it is not possible to reproduce the experimental data given by different symbols by theoretical models for the thermal neutron induced fission of ^{235}U. The experimental data show a too low neutron multiplicity at low TKE values and a too high neutron multiplicity at high TKE close to the Q-value of the reaction.

The new results using the detector system shown in Fig. 9 are presented in Fig. 11 again compared to the available literature data. It is clear that the new results (black full points) [20] solve the issue with the too high neutron multiplicity at high TKE and also the too low neutron multiplicity at low TKE. The slope of the distributions given in Fig. 11 is quite different to the one using the pervious literature data. This slope is a measure of the energy cost to emit an additional neutron. More details can be found in Ref. [20].

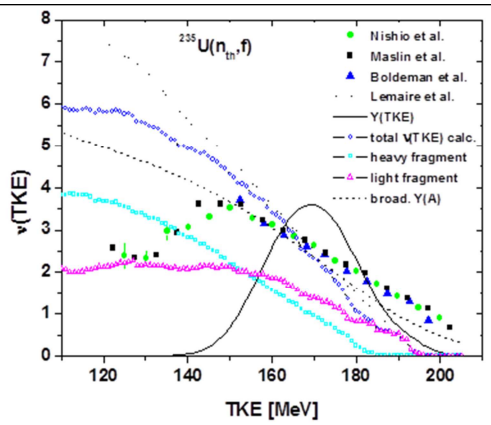

Fig. 10. Neutron multiplicity as a function of TKE for ^{235}U(n$_{th}$,f). A comparison is made to present literature data and theoretical calculations. Image taken from Ref. [19].

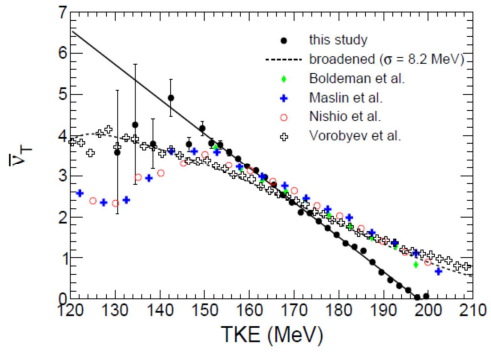

Fig. 11. Neutron multiplicity as a function of TKE for ^{235}U(n$_{th}$,f). A comparison is made to present literature data. Image taken from Ref. [20].

The reason for the difference between our most recent data [20] and literature is found in the comparison of the mass yield and TKE distributions as shown in Fig. 12.

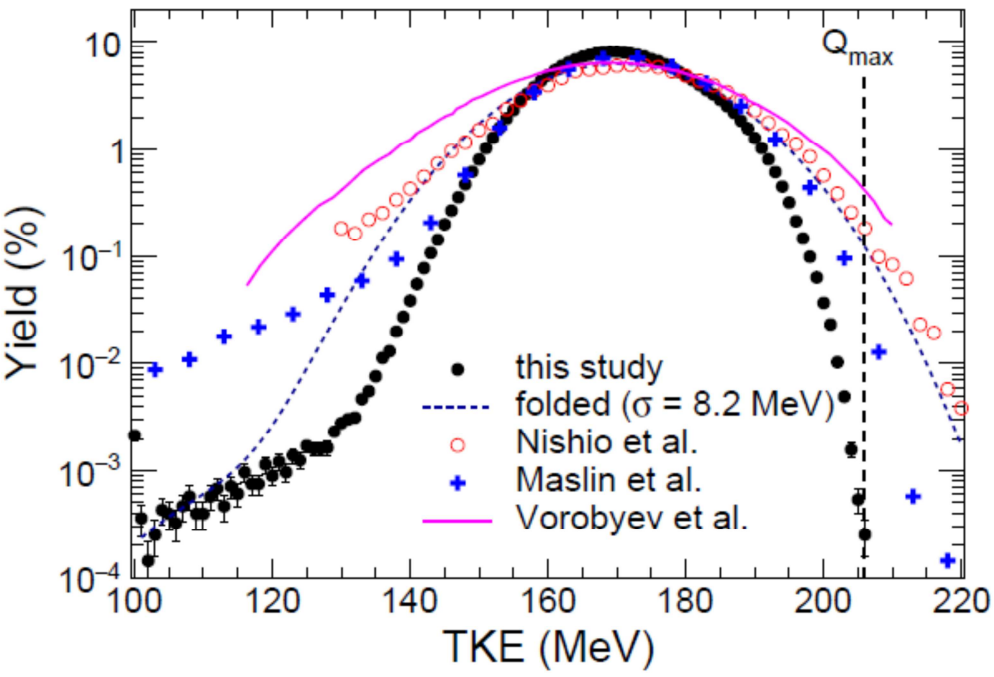

Fig. 12. Comparison of the fragment TKE distribution with literature data [21, 22, 23]. The dotted black line is the result obtained by folding the present data set with a Gaussian resolution function with σ = 8.2 MeV, necessary to reproduce the data of Nishio et al. [21]. The vertical dashed line labelled Q_{max} indicates the maximum available energy. Image taken from Ref. [20].

It is very obvious that previous literature data have a problem with a much too broad mass yield (not shown) and total kinetic energy distribution. If the present distribution (black full points) is artificially broadened by σ = 8.2 MeV, we barely can reproduce

the distribution of Nishio et al. [21], not to speak about the one of Vorobyev et al. [22]. It was only Maslin et al. [23] who mentioned problems with the resolution in their publication. All the three literature TKE distribution mentioned extent above the maximal Q-value of the reaction and show a strong tailing effect towards low TKE values. Since the neutron multiplicity is very dependent on the TKE value as shown in Fig. 11, it is clear that if the mass yield and TKE distributions are too broad also the neutron multiplicity as a function of mass and TKE have to be taken with very much caution.

Events belonging to the tailing or from above the Q-value as seen in Fig. 12 are likely due to scattering of the fission fragments in the target foil and/or surrounding materials. The neutron emission from such energy degraded fission events is expected to be close to the average value. This is consistent with the observed decrease in the neutron multiplicity at lower TKE as the tailing become more and more dominant in the yield as well as the levelling out at high TKE where the neutron multiplicity should drop to zero above the Q-value.

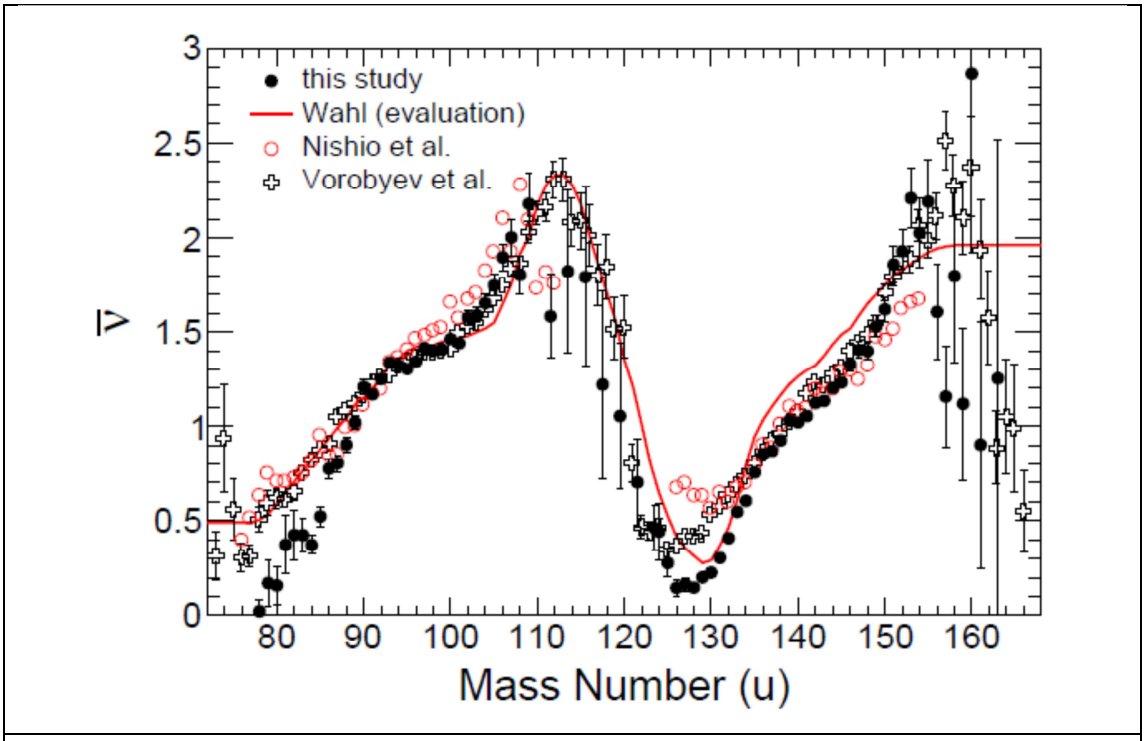

Fig. 13. The neutron multiplicity as a function of the fragment mass compared to data from Refs. [21, 22] and the evaluation by Wahl [24]. Image taken from Ref. [20].

The average neutron multiplicity as a function of the fragment mass is shown in Fig. 13. For comparison experimental data from Refs. [21, 22] and the evaluation from Ref. [24] are also show in the figure. The general shape is reproduced however the minima around mass number ~80 u for the light fragments and ~130 u for the heavy fragments appear more pronounced in the present data. This is a consequence of the higher resolution of the experiment of Ref. [20] compared to previous results as shown in Fig. 12.

Prompt fission γ-ray emission

As mentioned in the introduction fission fragment de-excitation takes place at a very early stage after scission. Prompt γ-ray emission is part of this de-excitation and was investigated essentially in the early 1970 years and only for a limited number of fissioning isotopes. This was done in view of nuclear applications as from the measured prompt fission γ-ray spectra (PFGS) average values for the total energy release per fission and γ-multiplicity were obtained, and used in evaluations.
The principal difficulty in prompt fission γ-ray measurements is the wide-spread time distribution, which covers the region from below picoseconds up to several microseconds. The obtained spectral data are, therefore, very sensitive to the particular experimental set-up, the covered time region as well as to the energy range of the emitted γ-rays. An inherent problem of such measurements is the sufficient discrimination of prompt fission neutrons, which may induce the production of γ-rays through inelastic scattering in the detector and the surrounding materials, mixing with the signal from prompt fission γ-rays.
As mentioned the systematic study of prompt fission γ-ray (PFG) emission started in the 1970 years. Several studies on spontaneous fission of ^{252}Cf [25] and thermal neutron-induced fission on ^{235}U [25–27], ^{233}U [27, 28] and ^{239}Pu [25, 28] were conducted. The energy range for γ-rays was from 10 keV [26] up to 8 MeV. All experiments were adapted in view of the flight path length with the timing resolution of the, at that time used, NaI γ-ray detectors. Time dependence of PFG emission was investigated up to 275 ns after fission [28], where the distinction from the neutron-induced γ-ray component becomes increasingly difficult. One reason is the limited pulse-height resolution of sodium-iodine based scintillation detectors, which do not allow a suppression of this component by pulse height analysis.

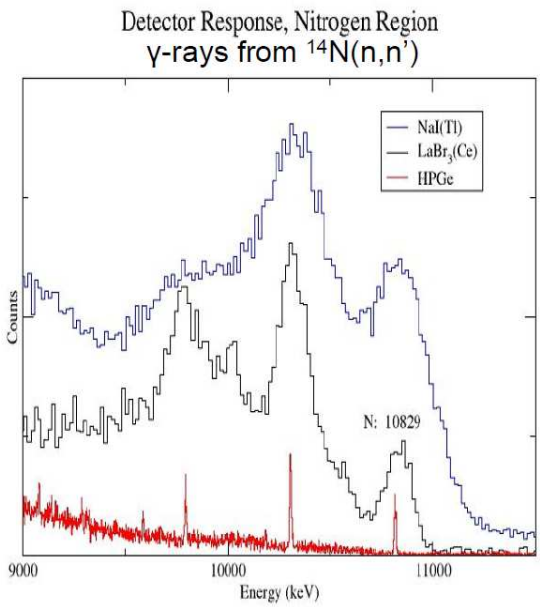

Fig. 14. Comparison of the resolution by different detectors, NaI (blue line), $LaBr_3$ (black line) and HPGe (red line). A clear difference is observed. Image taken from [33].

With the development of advanced Generation-IV nuclear reactors, also the need of new PFGS data became obvious. Since four out of six contemplated Generation-IV reactors require a fast neutron spectrum, a wider range of incident neutron energies

has to be considered [29]. Modeling of innovative core designs shows that, despite the numerous experiment campaigns reported in literature the data quality is not sufficient. The uncertainties attributed to the present PFG data, even for standard thermal power reactors, led to an under-prediction of the γ-heating by up to 30%, whereas an accuracy within 7.5% is requested. As a consequence urgent data requests were issued in the high-priority data request list (HPRL) of the OECD/NEA [30] for

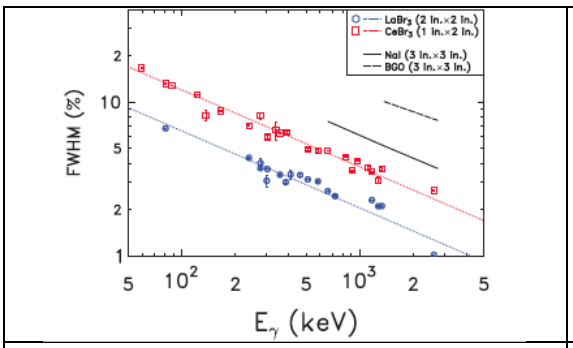

Fig. 15. Energy resolution of different lanthanide-halide detectors compared to BGO and NaI detectors. Image taken from [34].

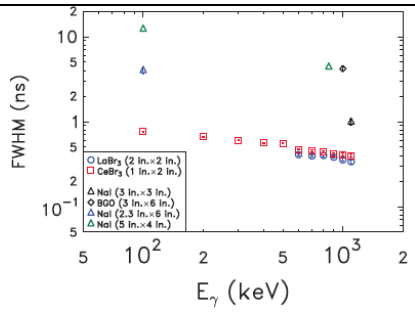

Fig. 16. Timing resolution of different lanthanide-halide detectors compared to BGO and NaI detectors. Image taken from [34].

the relevant isotopes ^{235}U and ^{239}Pu of today's thermal power reactors. Due to recent developments of new γ-ray detectors [31, 32] as well as digital data acquisition systems, the determination of new and improved PFGS characteristics became possible with high precision.

However, a major difficulty in such measurements is, apart from the need to obtain a sufficient mass resolution for fission fragments, the clear suppression of back-ground γ-rays induced by prompt fission neutrons in the γ-detector. The commonly used method is to discriminate γ-rays and neutrons by their different time-of-flight. This is strongly dependent on the timing resolution of the detector, which is normally not better than a few ns for NaI:Tl detectors as used in the past.

A solution to this problem is given by the recently developed lanthanum and cerium halide scintillation detectors, such as cerium-doped $LaCl_3$ and $LaBr_3$ as well as $CeBr_3$ detectors. The first two have shown to provide an intrinsic timing resolution well below 500 ps as well as an up to 60% better energy resolution compared to NaI, see Refs. [31, 32] and references therein. Also the efficiency of those detectors is significantly higher than NaI detectors of same size.

Another issue is the energy resolution. Fig. 14 shows a nice comparison between the energy resolution of a NaI(Tl), a cerium doped $LaBr_3$ and a HPGe detector. The latter has of course the best resolution but is very much neutron sensitive and its timing resolution is rather poor and even worse than for NaI detectors.

In Figs. 15, 16 a comparison of the energy and timing resolution is given for two different lanthanum-halide detectors compared to those obtained with NaI and Bismuth Germanium Oxide (BGO) detectors. Also here the improvement is very obvious.

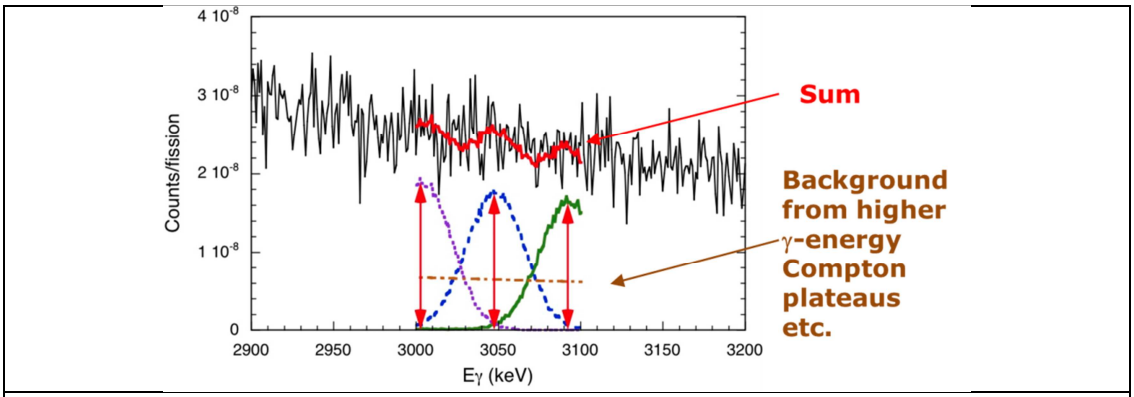

Fig. 17. Unfolding the detector response using the unfolding code PENELOPE [35].

But like in the case of the neutron detectors also the measured spectrum with the γ-ray detectors need to be unfolded according to the response function of the used detector. As photons of a given energy can have several interactions inside the detector crystal, i.e. Compton scattering and pair production, there is always a possibility that the photon escapes before it has deposited its full energy. To simulate this over the entire energy the Monte-Carlo code PENELOPE [35] has been used. Fig. 17 shows how this simulation is done. It takes into account the detector geometry, the geometric efficiency as well as different photon interactions that occur in the crystal. The accuracy of the simulation has been verified with calibration sources. In total 300 energies in the interval 100 keV up to 12 MeV have been simulated. Fig. 18 shows a comparison of the simulated spectrum with the measured one. The agreement is very good.

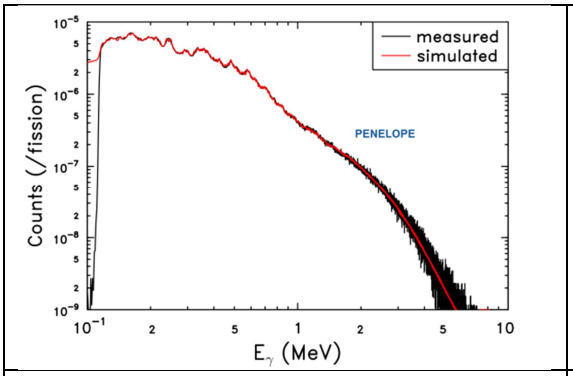

Fig. 18. Comparison of a measured versus a simulated spectrum.

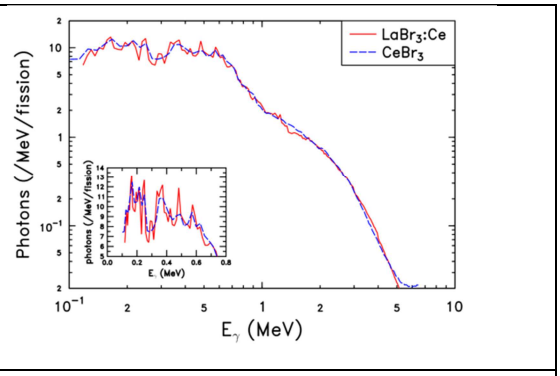

Fig. 19. Final prompt fission γ-ray spectrum of ^{252}Cf(sf).

Nevertheless it has been found that also more sophisticated simulations using the GEANT4 package [13] like for neutrons (see the previous chapter) is needed. GEANT4 has the possibility to include the full set-up geometry as backscatter of γ-rays from the set-up and the environment can be an important contribution to the measured spectrum as seen in Fig. 20 [36]. For different set-ups the backscatter peak region in the spectrum can be rather different with consequences on the unfolding of the measured spectrum.

The more elaborated simulation using GEANT and a realistic model of the experimental set-up like given in Fig. 21 leads to a much better reproduction of the measured calibration spectrum as seen in Fig. 22 [36]. Especially the interior of the

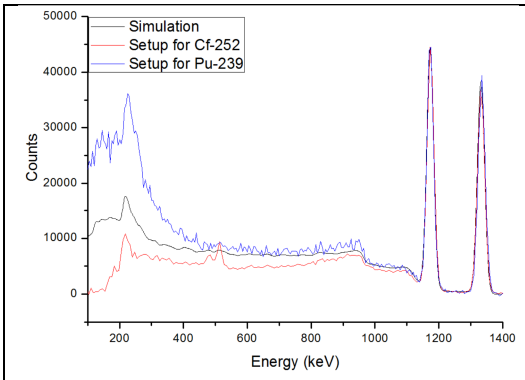

Fig. 20. Measured and simulated ^{60}Co spectra in three different experimental set-ups. Image taken from [36].

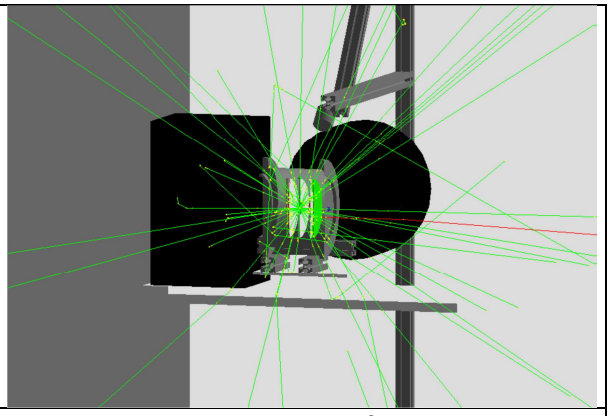

Fig. 21. Realistic setup of the experiment where multiple photon events are simulated shown by the green lines. Image taken from [36].

used ionisation chamber seem to have an unexpectedly large influence on the backscatter correction. Adding the cathode plate to the simulation resolved the issues observed with an increased backscatter peak as in Fig. 20.
The consequence of the improved unfolding is seen in Fig. 23. A better reproduction of the calibration spectra resulted in a better reproduction of the measured prompt fission gamma ray spectrum especially in the low energy part, say below 1 MeV.

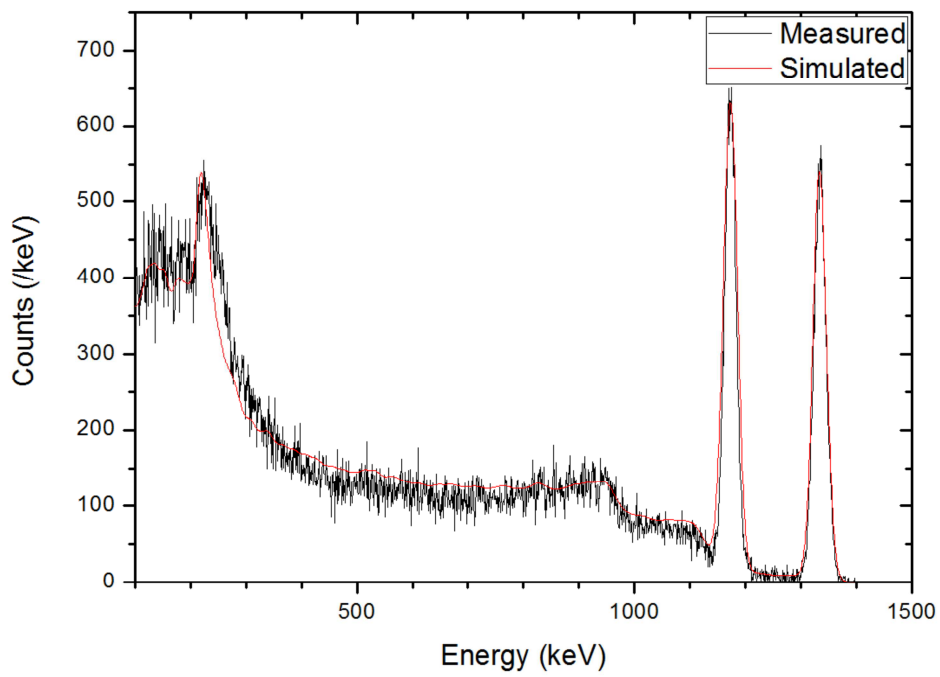

Fig. 22. Measured and GEANT4 simulated spectra for ^{60}Co. Image taken from [36].

Fig. 23 shows the comparison of the previously published PFGS for ^{235}U(n_{th},f) [37] (black line) with the one based on the improved simulation (red line) [36]. A clear reduction in yield below say 400 keV γ-ray energy is observed. The improved PFGS

is also now more in line with theoretical modelling with the code FIFRELIN of Ref. [38] in this low energy range.

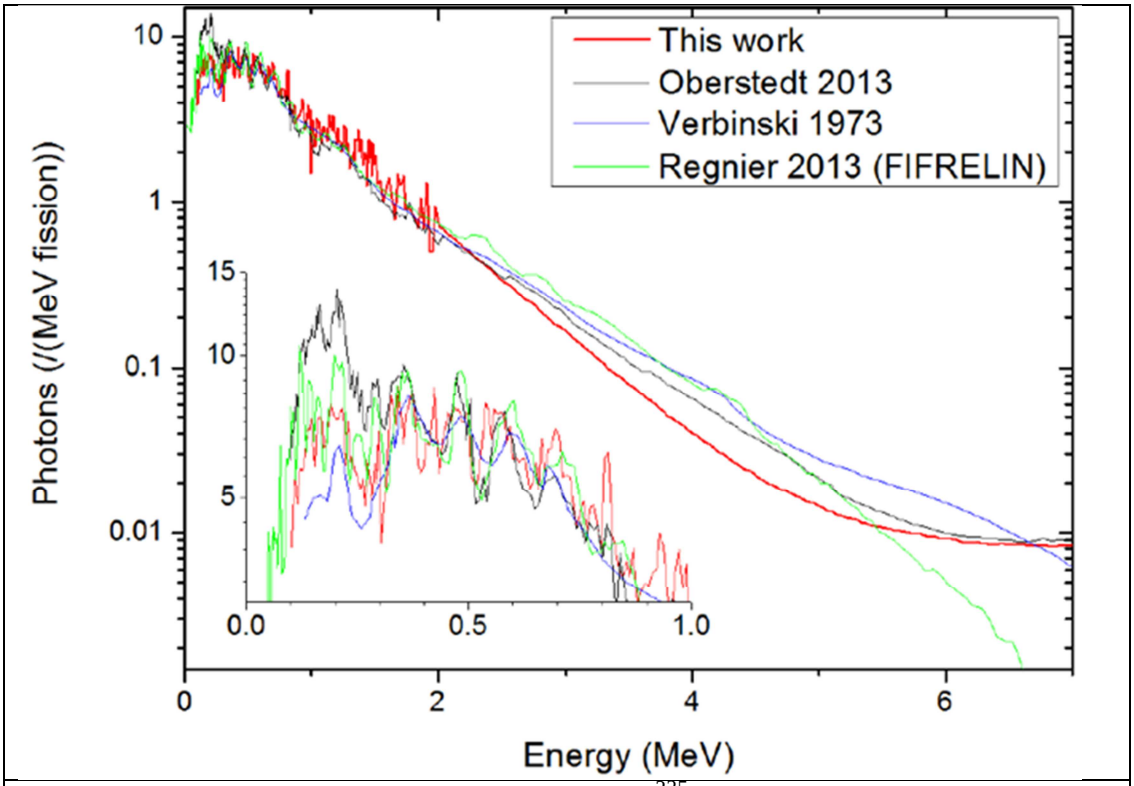

Fig. 23. Prompt fission γ-ray emission spectra of $^{235}U(n_{th},f)$ using the improved simulation compared to the previous measurements of Oberstedt et al. [37]. The spectra are also compared to a model calculation [38] and to historical data [25]. Image taken from Ref. [36].

Finally Fig. 24 shows the PFGS recently measured using the same technique to unfold the energy-dependent detector response to γ-rays from different fissioning systems. Only the low energy range is highlighted. In all the fissioning systems the low energy range shows lots of structure due to the apparent contribution of individual fission fragments. There is a clear tendency that the yield is increasing with an increase in mass of the compound system undergoing fission. The exception if $^{241}Pu(n_{th},f)$, where the effect of an improved backscatter correction has not yet been investigated.

In addition the results obtained using the $LaBr_3$:Ce detectors is in strong discrepancy of the results obtained by Ref. [40] using the DANCE detector at LANL (see Fig. 24). The Detector for Advanced Neutron Capture Experiments (DANCE) is a 4π array of 160 BaF_2 scintillator crystals designed to study neutron capture reactions. Via a similar unfolding procedure as mentioned before the PFGS has been determined as shown in Fig. 24 by the line. However it is clear from this comparison that the structure seen with the $LaBr_3$:Ce detectors is completely washed out as well is the threshold higher for DANCE. Hence the interpretation of the results will be also different in both cases.

A further elaboration of the interpretation of those spectra is out of the scope of this paper and the reader is pointed to the given references.

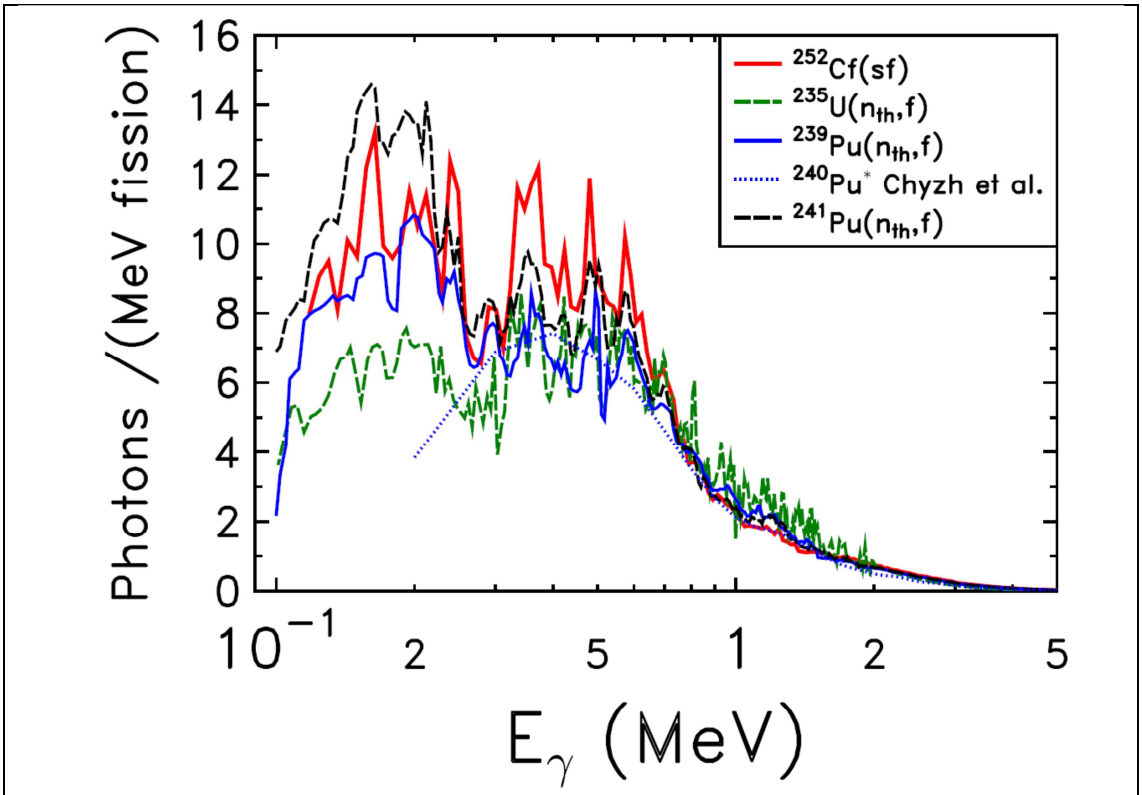

Fig. 24. Prompt fission γ-ray emission spectra taken with a $LaBr_3$:Ce after unfolding the energy-dependent detector response to γ-rays from different fission systems, ^{252}Cf(sf) [34]), ^{235}U(n_{th},f) [36] and ^{241}Pu(n_{th},f) [39]. The spectra are compared to a PFGS measurement of ^{252}Cf(sf) with an array of BaF_2 detectors [40].

Conclusions

The present paper discusses the investigation of prompt neutron and prompt γ-ray emission in fission. It is obvious that those measurements are very important both for understanding the fission process and for applications. The focus lies on high resolution measurements as well as very detailed simulations, resulting in superior quality of the correlations of fission fragments with prompt neutron and γ-ray emission. The new developments of detector systems with advanced characteristics for especially prompt γ-ray investigations have advanced the field. Very important as well is the use of digital data acquisition and digital signal processing.

References

[1] S. Oberstedt, A. Gatera, W. Geerts, A. Göök, F.-J. Hambsch, M. Vidali, A. Oberstedt, Rad. Phys. Chem. In press (2017)
[2] A. Riego, PhD thesis, UPC Barcelona Spain 2016
[3] X. Ledoux, J.-M. Laborie, P. Pras, I. Lantuéjoul-Thfoin, C. Varignon, Nucl. Instr. Meth. A 844 (2017) 24
[4] J. W. Boldeman, and M. G. Hines, Nucl. Sci. Eng. 91 (1985) 114
[5] R. Gwin, R. R. Spencer, and R. W. Ingle, Nucl. Sci. Eng. 87 (1984) 381
[6] D. A. Hicks, J. Ise, and R. V. Pyle, Phys. Rev. 101 (1956) 1016
[7] M. Dakowski, Y. A. Lazarev, V. F. Turchin, and L. S. Turovtse, Nucl. Inst. Meth.113 (1973) 195

[8] M. Soleilhac, J. Frehaut, and J. Gauriau, Journal of Nucl. Energy 23 (1969) 257
[9] B. Laurent, T. Granier, G. Bélier, A. Chatillon, J.-F. Martin, J. Taieb, F.-J. Hambsch, F. Tovesson, A.B. Laptev, R.C. Haight, R.O. Nelson, J.M. O'Donnell, Nucl. Instr. Meth. A745 (2014) 99
[10] G. Knoll, Radiation Detection and Measurement, 3rd Ed., (2000) John Wiley and Sons.
[11] A. Sardet, PhD thesis, U. Paris-Sud, France 2015
[12] A. Jančář, Z. Kopecký, J. Dressler, M. Veškrna, Z. Matěj, C. Granja, M. Solar, Rad. Phys. Chem. 116 (2015) 60
[13] GEANT4: A Simulation toolkit - GEANT4 Collaboration (Agostinelli, S. et al.) Nucl. Instr. Meth. A506 (2003) 250
[14] G. Dietze, H. Klein, Nucl. Instr. Meth. 193 (1982) 549
[15] C. Matei, F.-J. Hambsch, S. Oberstedt, Nucl. Instr. Meth. A 676 (2012) 135
[16] N.V. Kornilov, I. Fabry, S. Oberstedt, F.-J. Hambsch, Nucl. Instr. Meth. A 599 (2009) 226
[17] Chi-nu setup, https://e-reports-ext.llnl.gov/pdf/844505.pdf
[18] A. Göök, W. Geerts, F.-J. Hambsch, S. Oberstedt, M. Vidali, Sh.Zeynalov, Nucl. Instr. Meth. A830 (2016) 366
[19] N.V. Kornilov, F.-J. Hambsch, A.S. Vorobyev, Nucl. Phys. A789 (2007) 55
[20] A. Göök, F.-J. Hambsch, S. Oberstedt, Proceedings ND2016 in preparation
[21] K. Nishio, Y. Nakagome, H. Yamamoto, I. Kimura, Nucl. Phys. A 632 (1998) 540
[22] A. Vorobyev, O. Shcherbakov, A. Gagarski,G. Val'ski, G. Petrov, EPJ Web of Conf. 8 (2010) 03004
[23] E.E. Maslin, A.L. Rodgers, W.G.F. Core, Phys. Rev. 164 (1967) 1520
[24] C. Wahl, Atomic Data and Nuclear Data Tables 39 (1988) 56
[25] V.V. Verbinski, H. Weber, R.E. Sund, Phys. Rev. C 7 (1973) 1173
[26] R.W. Peelle, F.C. Maienschein, Phys. Rev. C 3 (1971) 373
[27] F. Pleasonton, R.L. Ferguson, H.W. Schmitt, Phys. Rev. C 6 (1972) 1023
[28] F. Pleasonton, R.L. Ferguson, H.W. Schmitt, Phys. Rev. A 213 (1973) 413
[29] G. Rimpault, in Proceedings of the Workshop on Nuclear Data Needs for Generation IV, April 2005, edited by P. Rullhusen (World Scientific, Singapore, 2006) p. 46
[30] Nuclear Data High Priority Request List of the NEA (Req. ID: H.3, H.4), http://www.nea.fr/html/dbdata/hprl/hprlview.pl?ID=421 and http://www.nea.fr/html/dbdata/hprl/hprlview.pl?ID=422.
[31] R. Billnert, S. Oberstedt, E. Andreotti, M. Hult, G. Marissens, A. Oberstedt, Nucl. Instr. Meth. A 647 (2011) 94
[32] A. Oberstedt, S. Oberstedt, R. Billnert, W. Geerts, F.-J. Hambsch, J. Karlsson, Nucl. Instr. Meth. A 668 (2012) 14
[33] P. Guess, SPIE conference presentation, San Diego, CA, August 21-25 (2011)
[34] R. Billnert, F.-J. Hambsch, A. Oberstedt, and S. Oberstedt, Phys. Rev. C 87, 024601 (2013)
[35] PENELOPE-2011, OECD/NEA/NSC/DOC (2011) 5; https://oecd-nea.org/science/docs/2011/nsc-doc2011-5.pdf
[36] A. Gatera, PhD-thesis, U. Gent, Belgium, 2017
[37] A. Oberstedt, R. Billnert, S. Oberstedt, Nucl. Instr. and Meth. A 708 (2013) 7
[38] D.Regnier, O. Litaize, and O. Serot, Phys Procedia 47 (2013) 47

[39] S. Oberstedt, R. Billnert, T. Belgya, T. Brys, W. Geerts, C. Guerrero, F.-J. Hambsch, Z. Kis, A. Moens, A. Oberstedt, G. Sibbens, L. Szentmiklosi, D. Vanleeuw, and M. Vidali, Phys. Rev. C 90, 024618 (2014).
[40] A. Chyzh, C.Y.Wu, E. Kwan, R.A. Henderson, J.M Gostic, T.A. Bredeweg, A. Couture, R.C. Haight, A. C. Hayes-Sterbenz, M. Jandel, H. Y. Lee, J. M. O'Donnell, and J.L. Ullmann, Phys. Rev. C 87, 034620 (2013).